Three-dimensional turbulence vorticity: Numerical and experimental modeling

D. Cano(^{1})(*), J. L. Cano(^{2}) and A. M. Matulka(^{3})(**)

(^{1}) *Instituto Nacional de Meteorología, Centro de Formación Madrid - Madrid, Spain*
(^{2}) *Facultad de CC. Físicas, Departamento de Astrofísica y Ciencias de la Atmósfera*
    Universidad Complutense de Madrid - Madrid, Spain
(^{3}) *Departamento de Física Aplicada, Universidad Politécnica de Catalunya*
    ETSECCPB - Barcelona, Spain

Summary. — We show in this paper how a system of equations of motion, diffusion and continuity that present the effects of vorticity through a vorticity transfer length scale may be used to model 2D-3D vorticity behaviour. The local turbulent vorticity is separated from the large-scale flow following the Reynolds decomposition (Reynolds 1894, Taylor 1931)—$\nabla \times \overline{v} + \nabla \times v'$—similar to the technique used for velocity. The system of equations extended through the terms $\nabla \times \overline{v}$ and $\nabla \times v'$ is solved numerically using a purely statistical local method that details the role of vorticity transport in the turbulence behaviour of the flow. Moreover, this numerical model that shows the temporal evolution of both fields, 3D velocity and 3D vorticity is used to investigate the propagation of turbulent perturbations that arise from the development of a vortex placed in the centre of the numerical domain. Even with a small mesh ($60 \times 60 \times 120$), the results show the propagation of vorticity-related waves both in the plane and in the vertical. The numerical results are compared with experiments performed in a stratified flow, where velocity and vorticity are measured with PIV as turbulence behind a grid decay, these experiments have been performed both in a rotating frame of reference and with no rotation and show features also detected in the numerical simulations when the assumption of a quasi–two-dimensional flow is used.

PACS `47.27.-i` – Turbulent flows.

1. – Introduction

Taking into account Taylor's proposal [1] that developed the concept of a turbulent exchange through the use of the rotational vector of velocity leading to a vorticity transfer length scale, in this work we have developed and expanded the concept used frequently

(*) E-mail: `dcano@inm.es`
(**) E-mail: `anna.magdalena.matulka@upc.edu`

in 2D turbulence to a full 3D system, and once we get the completed system of equations, it is possible to investigate the turbulence development, and in particular the role of the vorticity of a non-steady flow comparing a set of numerical solutions with laboratory experiments of similar conditions [2-4].

We have chosen a simple numerical solution of the system's finite integration, evaluating statistically the perturbations of the vorticity. In order to achieve this objective all the necessary equations of the vorticity have been simplified using an innovative way based on the vorticity transfer length-scales, and these have been solved for the large scales using a finite difference technique; including, the full three equations of motion (one for each component), an equation of applied diffusion for the development of energy and the equation of continuity based in the conservation of mass. The experiments study by means of detailed flow visualization and PIV the decay of a strongly stratified density interface (sometimes including rotation) after a grid traverses the interface. So both experiments and simulations model the first stages of decay of a quasi–two-dimensional flow. These types of turbulent flows under the effect of strong buoyancy (and in general body) forces are typical of geophysical flows, both in the ocean and the atmosphere.

The paper is organized in 6 sections as follows. After the introduction, sect. **2** shows the system of equations of motion based on 3D vorticity. In sect. **3**, we present the laboratory experiments. In sect. **4**, the numerical simulations are described and the results presented. In sect. **5**, we describe and discuss the main characteristics of the experimental and numerical behaviour of vorticity. In sect. **6** finally we present our conclusions comparing the numerical model and experiments and the most important results of this work are summarized.

2. – Equations of vorticity

We propose directly the system of equations of motion starting from the classical concept of vorticity, *i.e.* the velocity curl that we can write in vector form as

$$\overline{\xi} = \nabla \times \overline{v},$$ (1)

$\overline{\xi}$ and $\overline{v}$ being vorticity and velocity vectors, respectively. We will use, for simplicity of expression, the following boldface notations for vectors $\overline{\xi} = \boldsymbol{\xi}$ and $\overline{v} = \mathbf{v}$, $\boldsymbol{\xi} = (\zeta, \eta, \xi)$ and $\mathbf{v} = (u, v, w)$ being the vectors and their corresponding components for vorticity and velocity, respectively [1,5].

Analytically, the relation that exists between both vectors in a Cartesian frame of reference is

$$\boldsymbol{\xi} = \left(\frac{\partial w}{\partial y} - \frac{\partial v}{\partial z}\right)\mathbf{i} + \left(\frac{\partial u}{\partial z} - \frac{\partial w}{\partial x}\right)\mathbf{j} + \left(\frac{\partial v}{\partial x} - \frac{\partial u}{\partial y}\right)\mathbf{k}.$$ (2)

Retaking the hypothesis of Reynolds [6], decomposing the flow in mean and fluctuations and applying it to vorticity vector we can write for turbulent flows:

$$\boldsymbol{\xi} = \overline{\boldsymbol{\xi}} + \boldsymbol{\xi}'$$ (3)

$\boldsymbol{\xi}$ being the vorticity vector, $\overline{\boldsymbol{\xi}}$ the average vorticity vector and $\boldsymbol{\xi}'$ the turbulent perturbation of the vorticity vector. Starting from now $\overline{\boldsymbol{\xi}}$ is going to be interpreted as the average

rotation with which a turbulent eddy would be developed. $\boldsymbol{\xi}$ is the rotation that the turbulent flow imposes for each of the elements of flowing volume that they constitute it. Therefore $\boldsymbol{\xi}'$ is the difference between the actual (and instantaneous) rotation and the average rotation of the fore mentioned eddy. $\boldsymbol{\xi}'$ is going to be identified as turbulent vorticity from now on following Taylor and more recently Holzäpfel *et al.* [1, 7].

If we use this kind of decomposition to the different components of vorticity vector, we obtain

(4) $$\boldsymbol{\xi} = \left(\overline{\zeta} + \zeta', \overline{\eta} + \eta', \overline{\xi} + \xi' \right),$$

where (ζ, η, ξ) are the three components mentioned on the (x, y, z) axes, respectively.

Using the corresponding algebra to average values and derivatives it is possible to prove easily the relations that exist among the average and perturbed components of the vorticity vector and the corresponding velocity vector components:

$$\overline{\zeta} = \left(\frac{\partial \overline{w}}{\partial y} - \frac{\partial \overline{v}}{\partial z} \right),$$

$$\overline{\eta} = \left(\frac{\partial \overline{u}}{\partial z} - \frac{\partial \overline{w}}{\partial x} \right),$$

$$\overline{\xi} = \left(\frac{\partial \overline{v}}{\partial x} - \frac{\partial \overline{u}}{\partial y} \right),$$

for the average components and

$$\zeta' = \left(\frac{\partial w'}{\partial y} - \frac{\partial v'}{\partial z} \right),$$

$$\eta' = \left(\frac{\partial u'}{\partial z} - \frac{\partial w'}{\partial x} \right),$$

$$\xi' = \left(\frac{\partial v'}{\partial x} - \frac{\partial u'}{\partial y} \right),$$

for the fluctuating ones.

As an example, we can see the way to obtain the first component:

(5) $$\zeta' = \zeta - \overline{\zeta} = \left(\frac{\partial w}{\partial y} - \frac{\partial v}{\partial z} \right) - \left(\frac{\partial \overline{w}}{\partial y} - \frac{\partial \overline{v}}{\partial z} \right) = \left(\frac{\partial (w - \overline{w})}{\partial y} - \frac{\partial (v - \overline{v})}{\partial z} \right)$$
$$= \left(\frac{\partial w'}{\partial y} - \frac{\partial v'}{\partial z} \right),$$

and the same for the other two components. When we consider a turbulent flow developed in isotropic conditions, then we may impose to the three perturbed components of velocity vector, the condition

$$u' = v' = -w'.$$

Of course this condition could take place in a geophysical, ocean or atmospheric flow, only when we are located far from the generators of thermal or mechanical turbulence, *i.e.* far from ground, and if body forces are negligible. Using this isotropy expression and operating we deduce

(6)
$$\zeta' = \left(\frac{\partial w'}{\partial y} - \frac{\partial v'}{\partial z}\right) = \left(\frac{\partial(-u')}{\partial y} - \frac{\partial u'}{\partial z}\right),$$
$$\eta' = \left(\frac{\partial u'}{\partial z} - \frac{\partial w'}{\partial x}\right) = \left(\frac{\partial u'}{\partial z} - \frac{\partial(-u')}{\partial x}\right),$$
$$\xi' = \left(\frac{\partial v'}{\partial x} - \frac{\partial u'}{\partial y}\right) = \left(\frac{\partial u'}{\partial x} - \frac{\partial u'}{\partial y}\right)$$

and operating further we are able to show a new characteristic of the perturbed components of vorticity vector in isotropy and no body force situations:

(7)
$$\zeta' + \eta' - \xi' = 0 \rightarrow \zeta' + \eta' = \xi'.$$

So that the vorticity fluctuations are related in a similar way as found by Taylor [1]. All of the basic expressions presented until now would admit the inclusion of other assumptions from other generalized turbulent hypothesis equivalent to the theories, *e.g.*, or the theory of mixing length or those of variable coefficients of interchange.

In order to develop a more realistic system of equations of motion in which we are able to consider included the effect of the turbulent vorticity we can use as a starting point the equation of an ideal fluid and then add the corresponding terms associated to the forces or tensions of the physical effects to be modelled.

In this way if we apply the rotational operator to the Navier-Stokes equation we will obtain the vorticity equation with no body forces:

(8)
$$\frac{\mathrm{d}\boldsymbol{\xi}}{\mathrm{d}t} = \nabla P \times \nabla\left(\frac{1}{\rho}\right) + \boldsymbol{\xi} \cdot \nabla\mathbf{v} - \boldsymbol{\xi}\,\mathrm{div}\,\mathbf{v}.$$

If we did not include the viscosity effect ($\tau = \mu\nabla u$), we would obtain the equation of the simplest motion of a fluid. An optimal simplification of this equation to an ideal fluid would be the geostrophic equation

$$\frac{\mathrm{d}\mathbf{v}}{\mathrm{d}t} = -\frac{1}{\rho}\nabla P.$$

These equations allow us to write a new form of the equations of motion through the use of the explicit use of the kinetic energy and vorticity:

$$\frac{\partial u}{\partial t} + \frac{1}{2}\frac{\partial}{\partial x}\left(u^2 + v^2 + w^2\right) + w\eta - v\xi = -\frac{1}{\rho}\frac{\partial P}{\partial x},$$
$$\frac{\partial v}{\partial t} + \frac{1}{2}\frac{\partial}{\partial y}\left(u^2 + v^2 + w^2\right) + u\xi - w\zeta = -\frac{1}{\rho}\frac{\partial P}{\partial y},$$
$$\frac{\partial w}{\partial t} + \frac{1}{2}\frac{\partial}{\partial z}\left(u^2 + v^2 + w^2\right) + v\zeta - u\eta = -\frac{1}{\rho}\frac{\partial P}{\partial z}.$$

If we again consider the O. Reynolds enlargement to vorticity we can now write

$$\frac{\partial \overline{u}}{\partial t} + \frac{\partial}{\partial x}\left(\overline{E_c}\right) + \frac{\partial}{\partial x}\left(\overline{E_c'}\right) + \overline{w}\overline{\eta} + \overline{w'\eta'} - \overline{v}\overline{\xi} - \overline{v'\xi'} = -\frac{1}{\rho}\frac{\partial P}{\partial x},$$

$$\frac{\partial \overline{v}}{\partial t} + \frac{\partial}{\partial y}\left(\overline{E_c}\right) + \frac{\partial}{\partial y}\left(\overline{E_c'}\right) + \overline{u}\overline{\xi} + \overline{u'\xi'} - \overline{w}\overline{\zeta} - \overline{w'\zeta'} = -\frac{1}{\rho}\frac{\partial P}{\partial y},$$

$$\frac{\partial \overline{w}}{\partial t} + \frac{\partial}{\partial z}\left(\overline{E_c}\right) + \frac{\partial}{\partial z}\left(\overline{E_c'}\right) + \overline{v}\overline{\zeta} + \overline{v'\zeta'} - \overline{u}\overline{\eta} - \overline{u'\eta'} = -\frac{1}{\rho}\frac{\partial P}{\partial z},$$

where $\overline{u}$, $\overline{v}$, $\overline{w}$ are the three components of velocity vector; $\overline{\zeta}$, $\overline{\eta}$, $\overline{\xi}$ are the three components of the average vorticity vector; $\overline{E_c}$ the average kinetic energy of motion; u', v', w' the three perturbed components of velocity vector; ζ', η', ξ' the three perturbed components of vorticity vector; $\overline{E_c'}$ the average of the perturbed kinetic energy, that is to say $\frac{1}{2}(\overline{u'^2} + \overline{v'^2} + \overline{w'^2})$ and P the pressure. Obviously $\overline{u'} = 0$ although $\overline{u'^2} \neq 0$. We have to remember we are working with some fundamental simplifications, for example not considering effects such as buoyancy or Coriolis force effects, except possibly in their geometrical effects (2D topology).

If we now consider steady mean flow and such coordinates system that $\overline{\mathbf{v}} = (\overline{u}, 0, 0)$, the previous system is simplified to

$$\frac{\partial}{\partial x}\left(\overline{E_c}\right) + \frac{\partial}{\partial x}\left(\overline{E_c'}\right) + \overline{w'\eta'} - \overline{v'\xi'} = -\frac{1}{\rho}\frac{\partial P}{\partial x},$$

$$\frac{\partial}{\partial y}\left(\overline{E_c}\right) + \frac{\partial}{\partial y}\left(\overline{E_c'}\right) + \overline{u}\overline{\xi} + \overline{u'\xi'} - \overline{w'\zeta'} = -\frac{1}{\rho}\frac{\partial P}{\partial y},$$

$$\frac{\partial}{\partial z}\left(\overline{E_c}\right) + \frac{\partial}{\partial z}\left(\overline{E_c'}\right) + \overline{v'\zeta'} - \overline{u}\overline{\eta} - \overline{u'\eta'} = -\frac{1}{\rho}\frac{\partial P}{\partial z};$$

in the same way, if we use again the coordinate system and $\overline{u} = \overline{u}(y, z)$ (usual in meteorological condition),

$$\frac{\partial}{\partial x}\left(\overline{E_c'}\right) + \overline{w'\eta'} - \overline{v'\xi'} = -\frac{1}{\rho}\frac{\partial P}{\partial x},$$

$$\frac{\partial}{\partial y}\left(\overline{E_c'}\right) + \overline{u}\frac{\partial \overline{u}}{\partial y} + \overline{u}\overline{\xi} + \overline{u'\xi'} - \overline{w'\zeta'} = -\frac{1}{\rho}\frac{\partial P}{\partial y},$$

$$\frac{\partial}{\partial z}\left(\overline{E_c'}\right) + \overline{u}\frac{\partial \overline{u}}{\partial z} + \overline{v'\zeta'} - \overline{u}\overline{\eta} - \overline{u'\eta'} = -\frac{1}{\rho}\frac{\partial P}{\partial z}.$$

Finally, in vector form we can write

$$(9) \qquad \nabla\left(\overline{E_c'}\right) + \nabla\overline{\mathbf{v}}\cdot\overline{\mathbf{v}} + \overline{\boldsymbol{\xi}}\times\overline{\mathbf{v}} + \overline{\boldsymbol{\xi'}\times\mathbf{v'}} = -\frac{\nabla P}{\rho},$$

or

$$(10) \qquad \nabla\left(\overline{E_c'}\right) + \overline{\mathbf{v}}\nabla\overline{\mathbf{v}} + \overline{\boldsymbol{\xi'}\times\mathbf{v'}} = -\frac{\nabla P}{\rho}.$$

From eq. (9) another development is possible with the non-linear terms and similar conditions of the flow and coordinate system selected, that is $\overline{\mathbf{v}} = (\overline{u}, 0, 0)$, just as we show:

$$(11) \qquad \frac{\partial \overline{\mathbf{v}}}{\partial t} + \overline{\mathbf{v}} \cdot \nabla \overline{\mathbf{v}} = -\frac{1}{\rho} \nabla P - \overline{\mathbf{v}' \cdot \nabla \mathbf{v}'};$$

using the corresponding components of vectors we can write the next system:

$$(12) \qquad \frac{\partial}{\partial x}\left(\overline{u'u'}\right) + \frac{\partial}{\partial y}\left(\overline{u'v'}\right) + \frac{\partial}{\partial z}\left(\overline{u'w'}\right) = -\frac{1}{\rho}\frac{\partial \overline{P}}{\partial x},$$

$$\overline{u}\frac{\partial \overline{v}}{\partial x} + \frac{\partial}{\partial x}\left(\overline{v'u'}\right) + \frac{\partial}{\partial y}\left(\overline{v'v'}\right) + \frac{\partial}{\partial z}\left(\overline{v'w'}\right) = -\frac{1}{\rho}\frac{\partial \overline{P}}{\partial y},$$

$$\overline{u}\frac{\partial \overline{w}}{\partial x} + \frac{\partial}{\partial x}\left(\overline{w'u'}\right) + \frac{\partial}{\partial y}\left(\overline{w'v'}\right) + \frac{\partial}{\partial z}\left(\overline{w'w'}\right) = -\frac{1}{\rho}\frac{\partial \overline{P}}{\partial z}.$$

This system admits again the local isotropic hypothesis. According to that

$$(13) \qquad \overline{u'u'} = \overline{u'v'} = \overline{w'w'} = \overline{v'v'} = -\overline{v'w'} = -\overline{u'w'}.$$

Therefore, the system of eqs. (11) may be transformed to

$$(14) \qquad -2\overline{w'\frac{\partial u'}{\partial x}} - 2\overline{w'\frac{\partial u'}{\partial y}} + 2\overline{w'\frac{\partial u'}{\partial z}} = -\frac{1}{\rho}\frac{\partial \overline{P}}{\partial x}$$

$$\overline{u}\frac{\partial \overline{v}}{\partial x} - 2\overline{w'\frac{\partial u'}{\partial x}} - 2\overline{w'\frac{\partial u'}{\partial y}} + 2\overline{w'\frac{\partial u'}{\partial z}} = -\frac{1}{\rho}\frac{\partial \overline{P}}{\partial y}$$

$$\overline{u}\frac{\partial \overline{w}}{\partial x} + 2\overline{w'\frac{\partial u'}{\partial x}} + 2\overline{w'\frac{\partial u'}{\partial y}} - 2\overline{w'\frac{\partial u'}{\partial z}} = -\frac{1}{\rho}\frac{\partial \overline{P}}{\partial z}$$

One direct consequence of the last system would be

$$(15) \qquad -\frac{1}{\rho}\frac{\partial \overline{P}}{\partial x} = -\frac{1}{\rho}\frac{\partial \overline{P}}{\partial y} - \overline{u}\frac{\partial \overline{v}}{\partial x} = \frac{1}{\rho}\frac{\partial \overline{P}}{\partial z} + \overline{u}\frac{\partial \overline{w}}{\partial x}.$$

Finally through the components of turbulence vorticity we are able to propose the following system of equations in a turbulent flow relating velocity and vorticity components and pressure:

$$(16) \qquad 2\overline{w'(\xi' + \eta')} = -\frac{1}{\rho}\frac{\partial \overline{P}}{\partial x}$$

$$\overline{u}\frac{\partial \overline{v}}{\partial x} + 2\overline{w'(\xi' + \eta')} = -\frac{1}{\rho}\frac{\partial \overline{P}}{\partial y}$$

$$\overline{u}\frac{\partial \overline{w}}{\partial x} - 2\overline{w'(\xi' + \eta')} = -\frac{1}{\rho}\frac{\partial \overline{P}}{\partial z}$$

This system does not consider explicitly body forces, nor the anisotropy induced by them, but if we assume that small scales are not affected as much as the large scales
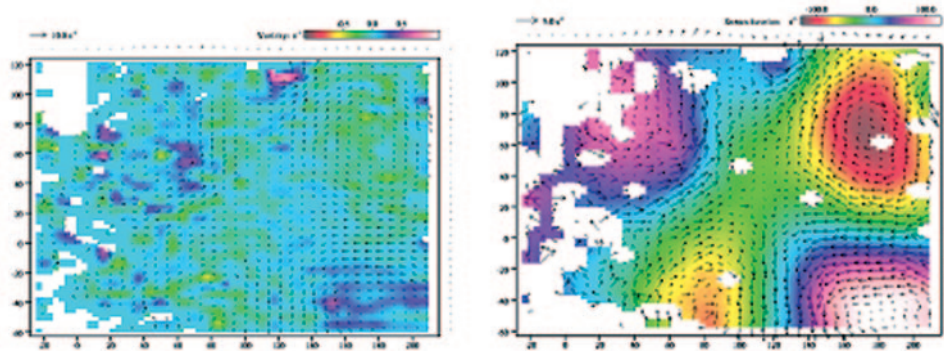
Fig. 1. – Evolution of a saddle structure in a rotating stirred flow, one of the characteristics of the flow is the development of strong vertical structures.

and force a vertical squashing in case of stable buoyancy, or a vertical elongation in case of fast rotation, other external forces may be considered locally using the limit of scales smaller than the Ozmidov or Hopfinger scales. It is important to investigate the topology of the flow, specially when non-homogeneous turbulence is produced by one or several body forces like buoyancy, rotation or magnetic fields [8-10]. The role of internal or inertial waves seems to affect the locality of the cascade processes. Arquimedes, Coriolis or Lorenz forces seem to produce changes in the scaling [11]. The fractal dimensions of the flows are related to the local Richardson, Ri, numbers [12, 13] and probably to the Rossby number Ro. A complex parametric space based on Re, Ri and $1/Ro$ is used to identify the dominant mixing instabilities and the vorticity structure.

These problems need further theoretical, numerical and observational work and one approach is to try to maximize the relevant geometrical information in order to understand and therefore predict these complex environmental flows.

3. – Laboratory experiments and results

A series of experiments have been performed on a strongly stratified two-layer fluid consisting of brine in the bottom and freshwater above in a 1 square meter tank. The evolution of the vortices after the passage of a grid is video recorded and particle tracking is applied on small pliolite particles floating at the interface. The combination of internal waves and vertical vorticity produces two separate time scales that may produce resonances. Here, results regarding the behaviour of the vorticity will be presented in simple conditions, results of the PIV laboratory experiments allow to calculate velocity spectra, the velocity and vorticity PDFs and the evolution of the structure of stratified (and rotating) decaying (and steady flows) as shown in fig. 1. One of the most important roles of stratification and rotation and in general of all body forces, including magnetic fields, is to modify the slope of the spectral energy cascade. While the anisotropy of the Reynolds stresses is obviously linked with the non-homogeneity and the body forces, acting mainly along the vertical axis (in stratified flows) and the rotation axis (in rotating flows). Scalar behaviour in such flows has non-linear mixing properties which are strongly influenced by the initial conditions [14, 8].

The set of experiments were performed on a square tank of dimensions $1\,\mathrm{m} \times 1\,\mathrm{m}$. Inside of this tank was a weight of $100\,\mathrm{kg}$ H_2O, distributed as $5\,\mathrm{cm}$ of salty water in the bottom and $5\,\mathrm{cm}$ of fresh water placed carefully with a sponge to avoid mixing. Between

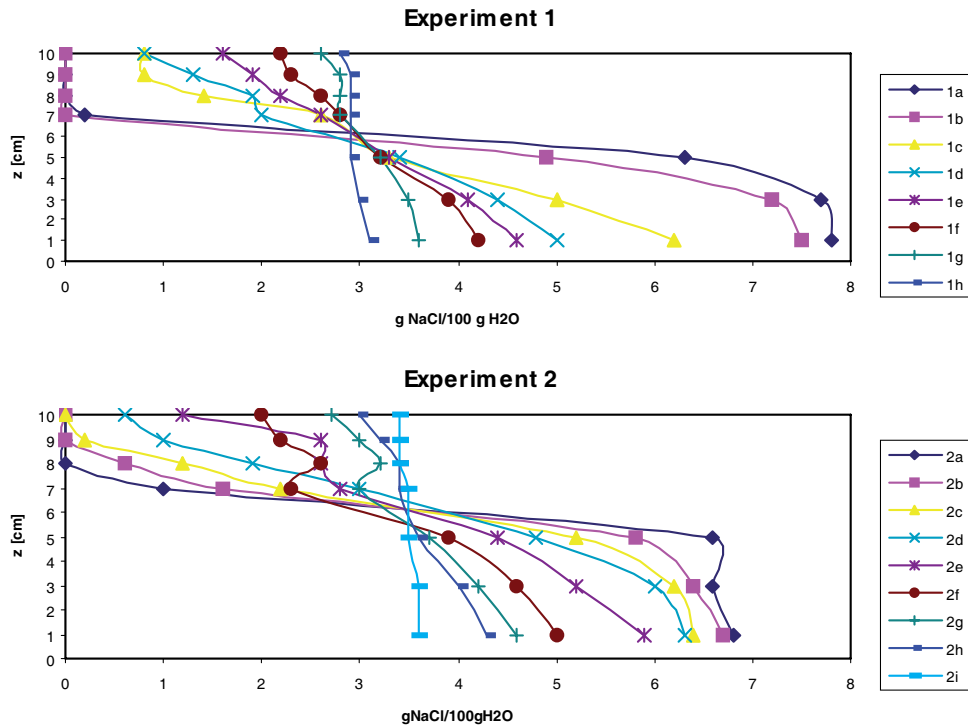**Experiment 1**

Experiment 2

Fig. 2. – Examples of the evolution of the density profiles after each passage of the grid in two laboratory experiments, when the density profiles are vertical, after several passages of the grid, then the two layers are completely mixed.

these two layers, the flow was seeded with a thin layer of tracer plastic particles of pliolite, marking the flow at the layer which separated the brine and fresh water. In order to mix these two layers a horizontally traversing grid was used, which was built from thick pipe sections (The bars were located every 10 cm, their length was 30 cm and their diameter 3.5 cm.) This configuration ensured strong vorticity produced by the Karman vortices of the round pipe array. This experiment had five subsets of different density interface experiments. In each one the measurements of the density profiles were obtained from point measurements at heights chosen as 1, 3, 5, 7, 8, 9, 10 cm of height inside the tank. Every experiment was made at different salinity in the brine fresh-water interface. Figure 2 shows the sequence of density profiles for experiments 1 and 2. The range of the initial gradient Richardson numbers of the 8 grid passages within experiment 1 was 8.8 to 0.039, while for the 9 passages in experiment 2 was 7.7 to 0.34. All small-scale measures had seven to nine profiles between the different passages of the grid. The mixing efficiency was measured between passages and it was related with the increase of potential energy and the decay process considering how long and how many grid passages were necessary for these two layers to be totally mixed. Individual turbulent decay processes combined to the overall mixing efficiency. In order to study the mixing process the grid was driven through the interface with the bars perpendicular to its plane and then we waited until all motions stopped. After this the densities were measured in the seven points, repeating the whole procedure again until in all the tank the density was the same, thus the two layers were totally mixed. See [13] for more information.
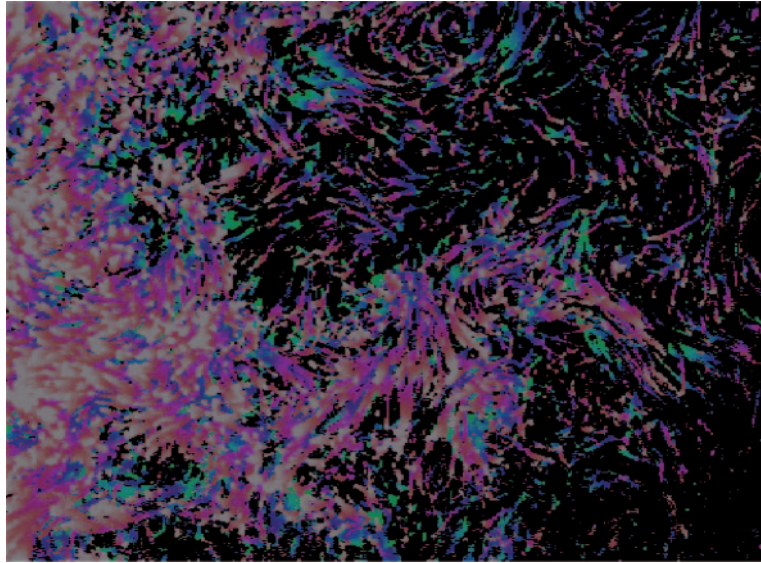
Fig. 3. – Pliolite particles and its traces 10 s after the passage of the grid perpendicularly to the centre of a sharp density interface.

In the entire set of experiments, the total mixing was dependent on the initial Richardson number. This difference shows a wide range of mixing efficiencies. The initial density difference at the fluid interface before mixing was in the limits between $1087 \lfloor \mathrm{kg/m^3} \rfloor \cong 8.7 \, [\mathrm{g\,NaCl}/100\,\mathrm{g\,H_2O}]$ and $1007 \lfloor \mathrm{kg/m^3} \rfloor \cong 0.7 \, [\mathrm{g\,NaCl}/100\,\mathrm{g\,H_2O}]$.

The values of the mixing efficiency are comparable with other experiments, but further
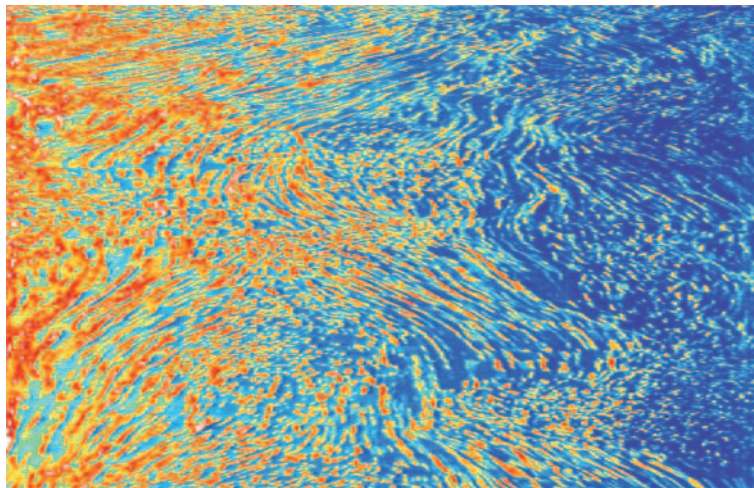
Fig. 4. – Evolution during 100 seconds of a column at the centre of the square tank as the stratified turbulence decays, the varying length scales are a measure of the dominant size of the vortices and the oscillations detected at different wavelengths are due to decaying internal waves at the interface.
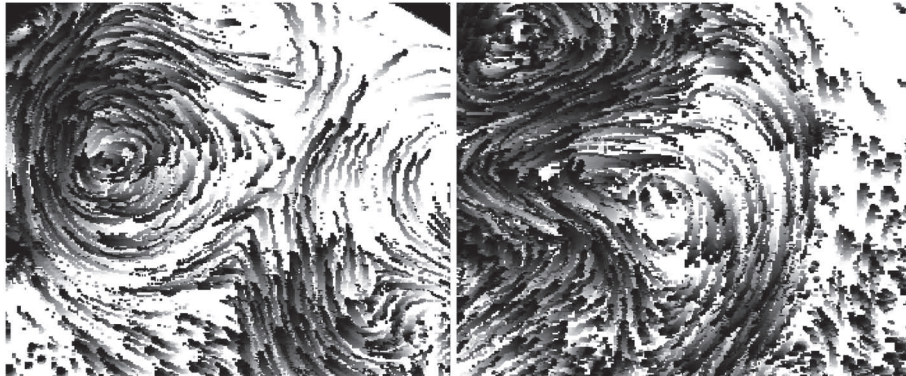
Fig. 5. – Example of particle tracking, following the pliolite tracers.

work is needed to investigate the effect of intermittency on the mixing process. This is still in progress [13, 15-17]. Examples of the flow visualization and PIV techniques used are shown in figs. 3 and 4.

Here we want to understand and describe key aspects of the structure of the non-homogeneous turbulence affected by stratification and rotation, in particular to study the evolution of the background vorticity and their interaction with the dominant coherent structures such as the dominant vortices. Other effects connected with non-homogeneity (for example, boundary layer-vortex interactions) are also studied. Figures 5 show particle traces detected at the density interface from above. There are several techniques that are used to track the pliolite particles and produce the velocity and vorticity plots used to calculate spatial correlations and spectra [13]. Figure 6 shows the evolution (during 1 second) of the vorticity (plane 2D) scalar field as the turbulence decays after the passage of the grid in the strongly stratified interface. The dominant vortices can be studied as they interact, merge or break up.

4. – Numerical simulation of the vorticity field

The numerical model used is detailed in [15-17]. The vorticity field is explicitly calculated using three integration regions so that at every time step the vorticity fluctuations are calculated statistically over a matrix of spatial and temporal grid points. The evolution of the vorticity is presented in time steps after the generation of a single vortex
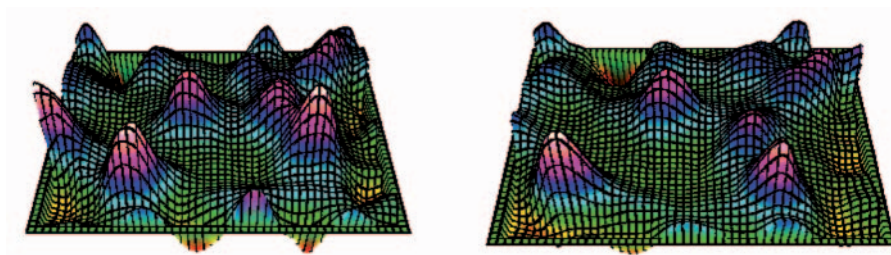

Fig. 6. – Example of 2D vorticity maps in false colour, the behaviour of the dominant vortices, seems much more complex than previously thought, showing non-local interactions.
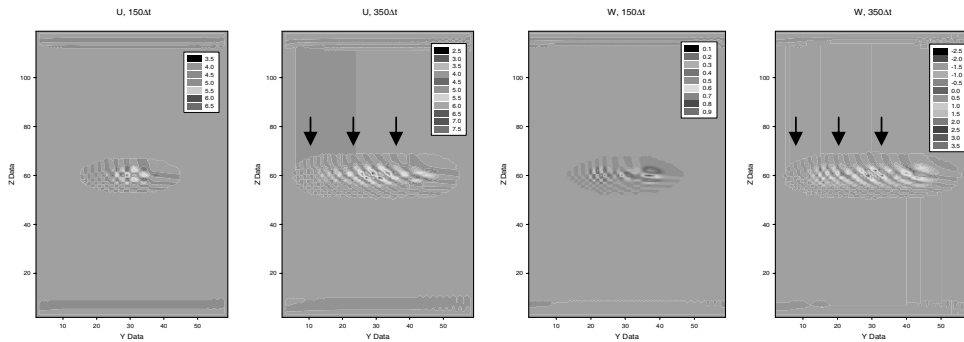
Fig. 7. – Temporal evolution of a single vortex placed in the centre of the domain. We show the first and third component of velocity for the moments of integration $150\Delta t$ and $350\Delta t$. Vorticity levels are shown in the figures.

in the centre of the domain. In fig. 7 comparison between graphs 150 and $350\Delta t$ for the first and third component of velocity evidences that the behaviour of the extreme values of both components is similar. In the meantime the growth of u comparing the initial velocity of the mesh, this is 5 units, reaches values of 6.5 units (30%) for $150\Delta t$ (same scale as for $250\Delta t$) and 7.5 units (50%) for $350\Delta t$. In the case of the vertical component w (starting from 0.5 units) quite low values of 0.9 (80%) for $150\Delta t$ come up to 3.5 units (700%) for $350\Delta t$. The model has to be considered even up to times of the order $400\Delta t$, mainly qualitative because the quantitative aspects do not agree well with the coherent evolutions and developments of the vortices within the 3 phases of the model. Nevertheless the evolution and overall growth of the vorticity patches is consistent with the experiments.
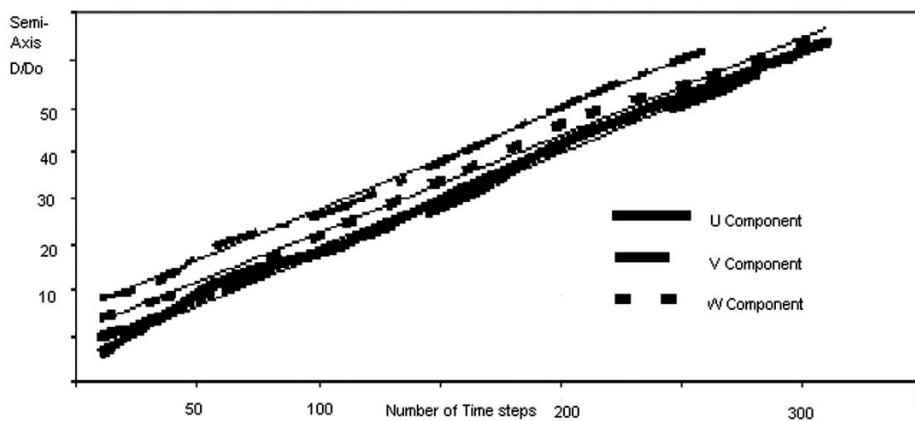

Fig. 8. – Linear fits for the growth of the horizontal coordinate y (elongation) of the size of the affected zone by the installed vortex at the centre of the mesh for the third phase of integration of the model. Fit variables: u, v, w and θ. The interior legend specifies the fit of every variable and their numerical parameters. We propose as greater semi-axis the elongation of the larger dimension (horizontal) of the zone. The size is measured with the number of affected cells and the time in Δt.
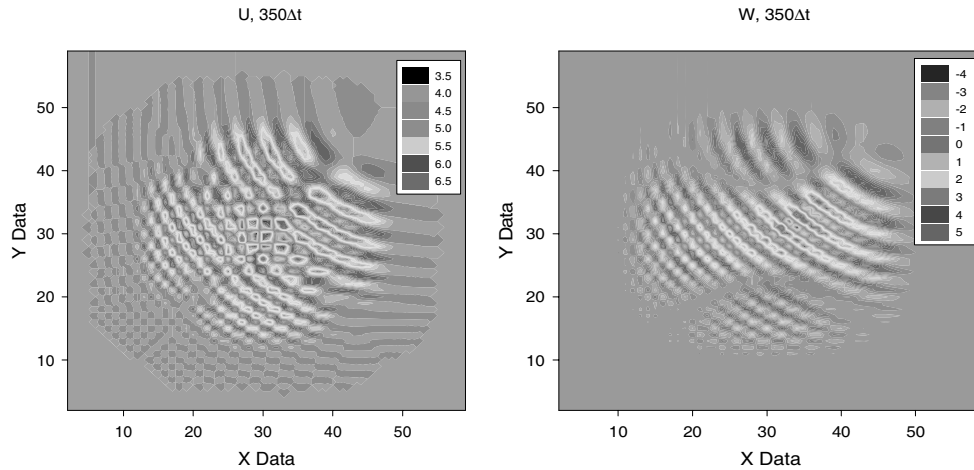
Fig. 9. – Temporal evolution of a vortex placed in the centre of the mesh. We show the u and w components of velocity in horizontal planes $z = 60$ for the moment of integration $350\Delta t$.

Figure 8 shows the temporal evolutions of the growth (elongation) of the zone of development of the vortex for the fields of the velocity components and the potential temperature (u, v, w and θ). It has been calculated from the linear fit at time steps of the calculations: 50, 75, 100, 150, 200, 250, 300 and $350\Delta t$ and we have chosen the size of the largest semi-axis (axis y) of the affected areas by the vortex in the vertical planes as indicative of the overall maximum size of the vortex. This result may be compared with [12]. We can visualize easily the elliptical aspect that 3D vorticity presents. We can observe the following aspects of a mainly isotropic vortex growth: the lines that show the growth of the vortex—fits of any of the four variables used in this study. The regression coefficients evidence that the selected fits present a high statistical reliability. It is remarkable the parallelism of the different lines of fit, indicating that the increase is practically the same for the four variables, presenting a nearly numerical value to 0.11 (slope of the straight lines), which corresponds to a 11% of relative expansion of the vortex. The independent terms of the different lines of fit differ lightly indicating with it that the beginning values for the elongation of the vortex are different according to the used variable. Let us remember that $K_{\rm h} > K_{\rm m}$ most of all for unstable stratification ($K_{\rm h}$ and $K_{\rm m}$ are the coefficients of turbulent viscosity for interchanges of heat and moment, respectively).

Figure 9 shows the comparison between the u and w components for the last few instants of integration and, therefore, for the last moments of development of the model in horizontal planes $z = 60$. The observable first thing is that the development in both axes is totally comparable and occupies the totality of the grid in its horizontal dimensions practically. The scales of the graphics do not allow showing the same zones for both variables. However, the quantitative direct observation of the numerical results of the model establishes at this advanced stage of the vortex evolution, the existence of wave-like disturbances. The figure shows the spatial development that initiates a subdivision of the space occupied by the variables u and w (also the rest of the variables) in several differentiated zones begins to be observable. In short we can observe four zones at these graphs and one intermediate transitional centred in 30×30 whose later evolution has not allowed to carry out an investigation because the model reaches greater dispersions for
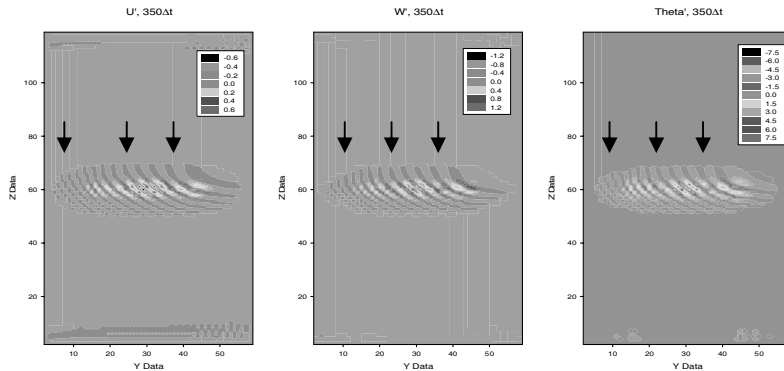
Fig. 10. – Temporal evolution of a vortex placed in the centre of the mesh. We show the turbulent perturbation of the first and third components of velocity and the potential temperature in vertical planes $x = 30$ for the moment of integration $350\Delta t$. The corresponding arrows indicate three differentiate zones.

later steps of integration. The observation of these four zones is justified because they are delimited by zones where the variables present a minimal alteration (and therefore close values to the points of the mesh not affected by the vortex).

Figure 10 shows the stage of integration reached for the $350\Delta t$ for the turbulent perturbations of the first and third components of velocity (u' and w') and of the potential temperature (θ'). Even though the w variation is large, presenting its turbulent perturbation of about 240% (w'), the turbulent perturbation to the potential temperature (θ') reaches only 2.5%, however the behaviours of w' and θ' should show more or less a good correlation. This implies clearly that the properties associated to mixing are observable, in these steps of integration at least qualitatively. The model, obviously, presents difficulty in the quantification of some phenomena because of the inevitable dispersion generated by the statistical contribution of many steps of integration.

The three plots of fig. 10 show, also, the division that has been commented so we can clearly differentiate three zones through the evolution and development of the variables u', w' and θ' of the vortex. Obviously these three zones, in the line $z = 60$, would correspond to the image of the line $x = 30$ in fig. 10.
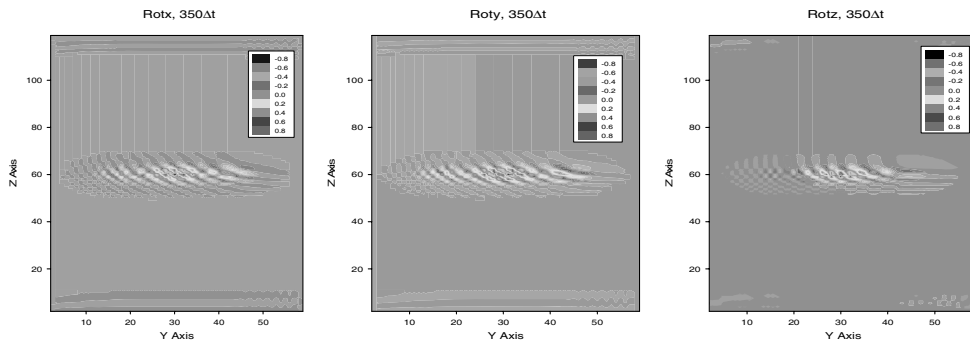

Fig. 11. – We show the three components of velocity curl (Rot$x$, Rot$y$ and Rot$z$) in the vertical planes $x = 30$ for the moment of integration $350\Delta t$.
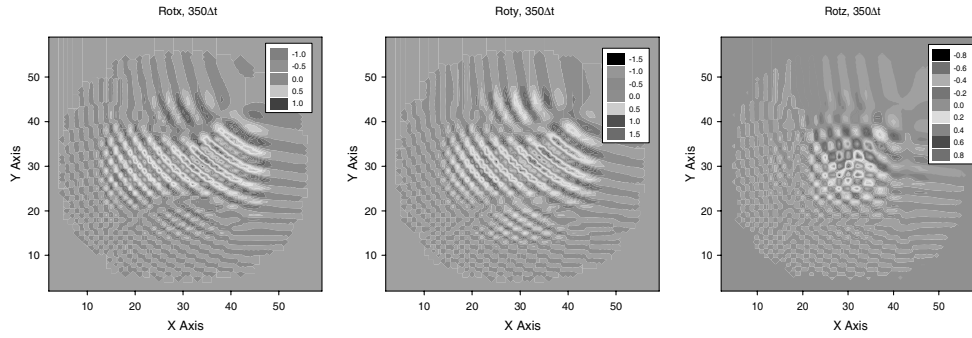
Fig. 12. – We show the three components of velocity curl (Rot$x$, Rot$y$ and Rot$z$) in horizontal planes $z = 60$ for the moment of integration $350\Delta t$.
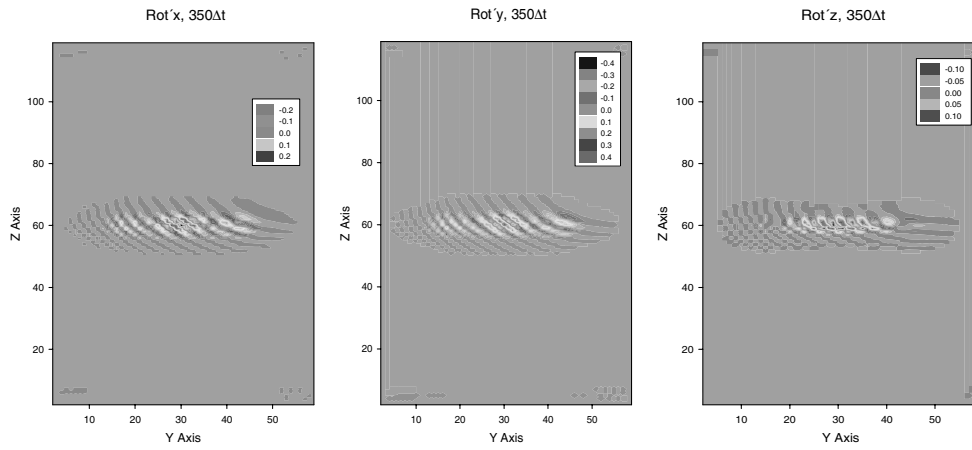

Fig. 13. – We show the turbulent perturbations of the three components of velocity curl (Rot$'x$, Rot$'y$ and Rot$'z$) in vertical planes $x = 30$ for the moment of integration $350\Delta t$.
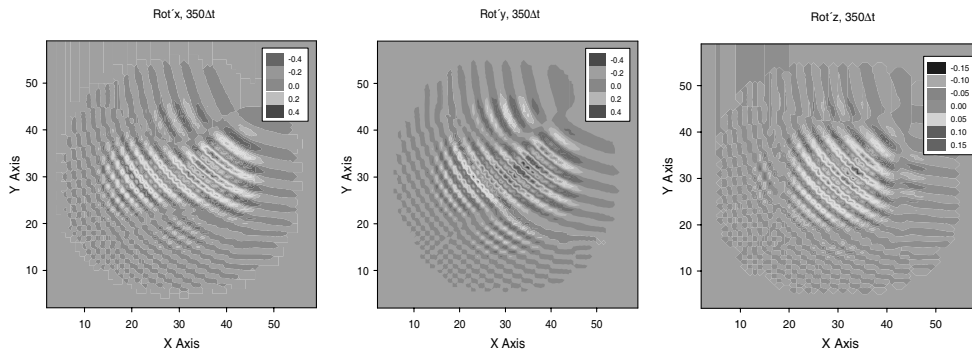

Fig. 14. – We show the turbulent perturbations of the three components of velocity curl (Rot$'x$, Rot$'y$ and Rot$'z$) in horizontal planes $z = 60$ for the moment of integration $350\Delta t$.
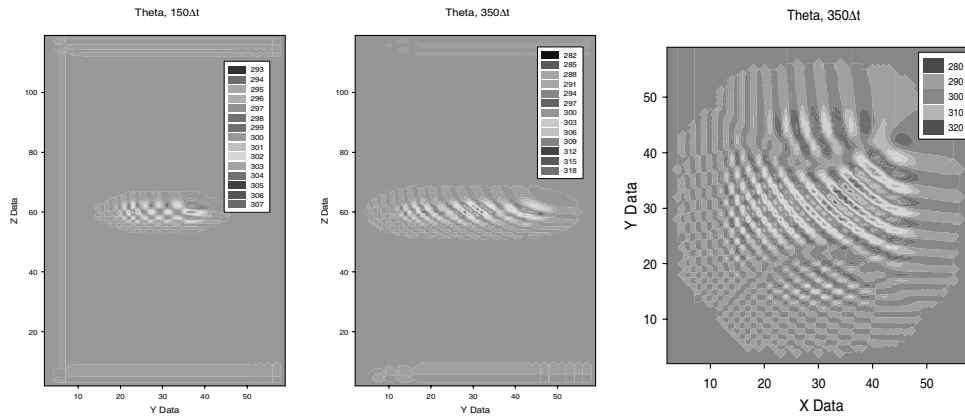
Fig. 15. – We show potential temperature in vertical planes $x = 30$ and horizontal planes $z = 60$ for the moments of integration $150\Delta t$ and $350\Delta t$.

Figures 11 to 14 show distributions of the three components of velocity curl and their turbulent perturbations for the instant $350\Delta t$. The corresponding graphics at the horizontal plane $x = 30$ inform of the elongation reached by the effect of the vortex expansion similar to that showed by the components of velocity and their turbulent perturbations. Although the three zones that have been used in other graphs are not superimposed they are easily observable.

The corresponding graphs to the horizontal planes $z = 60$ (figs. 12 and 14) show also similar developments and the partition of the influence zones at four sub-zones of possible different evolution with the exception of the third component of turbulent vorticity. This fact was anticipated because the x and y components of velocity curl join the space variations of the third component of velocity (the one that suffers greater alterations due to the numerical dispersion), meanwhile the third component of the turbulent vorticity is only influenced by the spatial variations of the first and second components of velocity, therefore their growth relation is not necessarily the same.

Figure 15 shows different instants for the evolution of the potential temperature in vertical and horizontal planes between times $150\Delta t$ and $350\Delta t$. The heat transport is associated to the general dynamic behaviour of the turbulent flow.

In fig. 16 we show as an example another type of results of the model of which we have selected only these four graphs. In the figure we see how the model analyzes
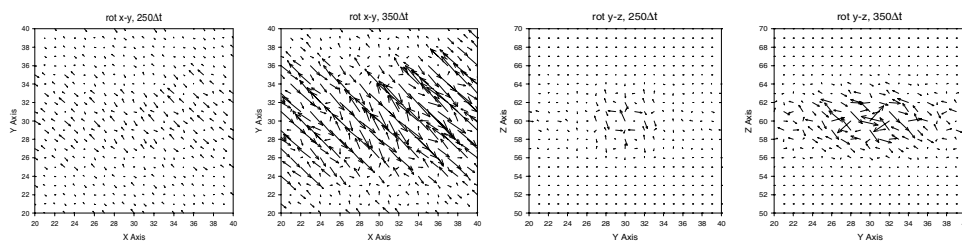

Fig. 16. – We show two instants of evolution ($250\Delta t$ and $350\Delta t$) of projection of the rotational vector on horizontal (Rot x-y) and vertical (Rot y-z) planes. Scale factor to the vectors is 1:2.
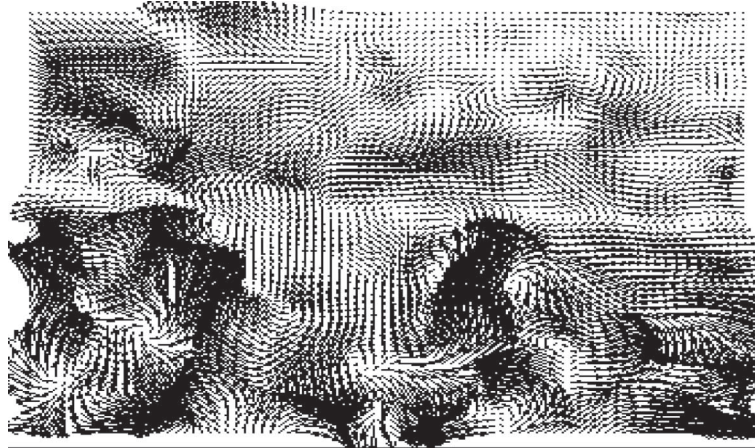
Fig. 17. – Vertical plane near a density interface showing the velocity vectors from a PIV showing the effect of the density interface on the reduction of the horizontal vorticity (Rot x-y).

the evolution and three-dimensional distribution of the component of the rotational vector of velocity. The observed alterations in the vectors of any of the four graphs are caused, logically, by the perturbations of velocity and rotational of velocity fields simultaneously.

It is possible to observe in the horizontal planes the irregularities or alterations produced by the behaviour of "rot x-y" from an altered situation in very centred bands close to $y = 30$ to other ones that they occupy most of the represented mesh in the graph of $350\Delta t$. Similarly the associated vectors to the x and y components of the vorticity imply opposite strong observable rotations in the case of very close vectors.

A parallel alignment of these rotations to second bisecting line of the drawn square $350\Delta t$ (rot x-y) is also observable. For vertical planes $x = 30$ (rot y-z) present the distribution of the projections in a vertical plane $x = 30$ of the second and third components of the rotational vector of velocity. For the instant $250\Delta t$ we find distributions for these rotations related to the rotations in perpendiculars planes to each one of them whose distribution centres in the line of $z = 60$ itself fundamentally and with modular values sufficiently developed but still small. In the instant $350\Delta t$ the band affected by these components show horizontal lines of development of the perturbation, we can observe also that in $250\Delta t$ perturbation values are closer to the centre of the mesh than at $350\Delta t$. Anyway we have to notice that horizontally it has not been intended to reach the maximum length of grid because as we have already indicated in the figures that show the $350\Delta t$ temporal interval the affected zone by the vortex occupies the totality of extension grid practically.

Figures 17, 18 and 19 show the velocity and vorticity plots obtained from the PIV analysis of the laboratory experiments, the flows are much more complicated than in the numerical simulations because instead of a single vortex evolution, the experiments represent the flow as the turbulence behind a grid decay, in order to simulate better the experimental flow, an array of vortices, such as those generated by a Karman vortex street behind an array of cylinders, would need to be introduced as initial conditions.
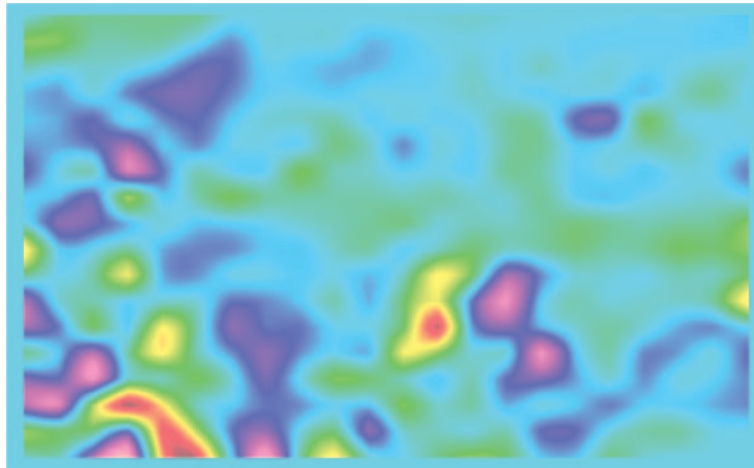
Fig. 18. – Vertical plane near a density interface showing the horizontal vorticity (Rot x-y).

5. – Discussion

On the one hand, for a stable stratification case it is clear that the behaviour of the vorticity vectors in a fully turbulent flow tends to align themselves with the vertical, even if the flow is not completely two dimensional, even if these 2D flows are an ideal limit, we may use the new conservation laws due to the reduction of one topological dimension to
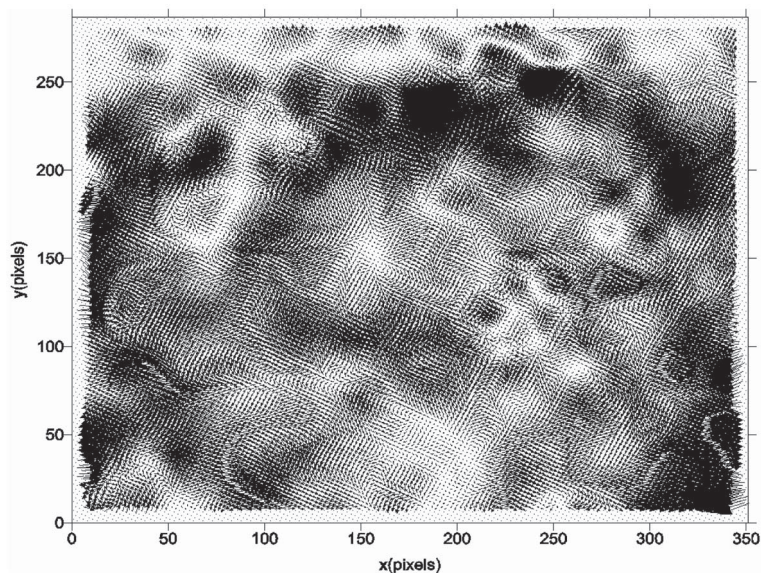

Fig. 19. – Large resolution PIV of a horizontal plane near a density interface showing the horizontal velocity field, the distribution of vortices as well as wave interactions are clearly detected.

explain and model the flat structure dynamics by random initial instabilities as precursors of quasi-2D or under the horizontal and vertical shear conservation arguments. There are still many arguments for or against an isotropic or an anisotropic and non-linear statistic theory of "wave-vortex" interactions, supported by direct numerical simulations and results of Lagrangian dispersion by passive tracers showing that diffusion looks dominated by the linear modes of movement, essentially anisotropic dispersive waves and the quasi-geostrophic modes, these interactions may even take place as a fractal-wave interactions [17, 18]. While the organized eddies from non-linear interactions play a minor role in the small-scale cascades the large eddies seem to dominate flows in the environment, specially when a 3D helicity component is present as in tornadoes, hurricanes, etc. Paradoxically the measurement of eddy structures is easy to visualize than the more elusive wave manifestations. The simulations presented in sect. **4**, however, show very clear the role of waves in the growth of vorticity patches. The reason is probably due to the full 3D simulation of the vorticity that does not constrain the growth of the nonrotational part of the velocity derivative tensor. In order to compare with the standard exact (but probably not real) pure 2D flow, we will discuss next the basic equations of the continuity and momentum, for an incompressible fluid, so that the continuity equation reduces to

$$(17) \qquad \Delta \cdot u = 0$$

and the equation of motion of an incompressible, homogeneous geophysical fluid with constant viscosity can be written as

$$(18) \qquad \frac{\partial u}{\partial t} + u_i \, \frac{\partial u}{\partial x_i} = -\frac{1}{\rho} \, \nabla p + \nabla \phi - 2\Omega * u + v\nabla^2 u,$$

where p is the pressure, ϕ the gravitational potential, Ω the angular velocity of Earth and ν kinematic viscosity. If the motion is primarily horizontal, then the flow is approximately two dimensional, *i.e.*

$$(19) \qquad \mathrm{v} = (u, v, 0),$$

where u, v are independent of depth. In a strictly 2D flow of this form there is only one non-zero component of vorticity (the vertical) and

$$(20) \qquad \xi = (0, 0, \xi).$$

In the absence of dissipation, vorticity is conserved

$$(21) \qquad \frac{\mathrm{D}\xi}{\mathrm{D}t} = 0$$

and this allows to define a stream function ψ so that

$$(22) \qquad u = \left(\frac{\partial \psi}{\partial y}, -\frac{\partial \psi}{\partial x}, 0 \right)$$

and

$$(23) \qquad \xi = -\nabla^2 \psi,$$

so the equation of vorticity conservation becomes

$$(24) \qquad \frac{\partial \xi}{\partial t} + J(\xi, \psi) = 0.$$

In strictly 2D flows with no dissipation we have conservation of energy

$$(25) \qquad \overline{u^2} = \int_0^\infty E(k,t)\mathrm{d}k$$

and of enstrophy

$$(26) \qquad \overline{\xi^2} = \int_0^\infty k^2\, E(k,t)\mathrm{d}k.$$

Conservation of enstrophy results from conservation of vorticity ξ (no stretching or twisting) but only if the viscous losses of vorticity are low enough. In flow (2D) but with weak dissipation the above results hold approximately. What is more interesting is to investigate the role of the most energetic vorticity peaks (or coherent structures) on the 2D or 3D velocity and vorticity cascades. From the experimental results it is clear that for real flows, eq. (26) is not exact, one of the possible reasons may be the role of viscosity in dissipating vorticity at the small scales, but another possibility is the non-local aspects of the most energetic vortices, as seen in fig. 6, that seem to interact in a different way.

The numerical model, even with a very small resolution may be used to investigate the role of wave-vortex interaction in turbulence. The basis of this study is the turbulent vorticity effects remarked and reinterpreted under Taylor's theory [1] for the different equations relating energy and vorticity in 3D. Once having obtained the system of equations shown in sect. **2**, the numerical integration performed shows new details of the evolution of one or several vortexes placed in the centre of the proposed numerical mesh.

A simplified equation system for the study of the almost 2D turbulence through an explicit calculation of the 3D small-scale vorticity, allows to evaluate the kinetic energy of the flow (throughout the Reynolds decomposition technique) leading to

$$\nabla\left(\overline{E'_c}\right) + \nabla\overline{\mathbf{v}} \cdot \overline{\mathbf{v}} + \overline{\boldsymbol{\xi}} \times \overline{\mathbf{v}} + \overline{\boldsymbol{\xi}' \times \mathbf{v}'} = -\frac{\nabla P}{\rho} \qquad \text{or} \qquad \nabla\left(\overline{E'_c}\right) + \overline{\mathbf{v}}\nabla\overline{\mathbf{v}} + \overline{\boldsymbol{\xi}' \times \mathbf{v}'} = -\frac{\nabla P}{\rho},$$

$\boldsymbol{\xi}$ being the vorticity vector. This tells us that there are significant contributions to the kinetic energy of the flow from the velocity-velocity gradient interactions, through the vorticity-velocity interactions both at mean and at fluctuation levels and finally from the pressure gradients that eventually lead to baroclinic vorticity.

The equation of continuity may also be used in the following form:

$$\frac{\partial \rho}{\partial t} = -\operatorname{div}\left(\rho \overline{\mathbf{v}}_{\mathrm{tr}}\right) - \left(\overline{\boldsymbol{\xi}} \times \mathbf{r}_c\right) \cdot \frac{\nabla \rho}{2} - \frac{\rho}{2}\operatorname{div}\left(\overline{\boldsymbol{\xi}} \times \mathbf{r}_c\right),$$

$\mathbf{v}_{\mathrm{tr}}$ being a translation velocity, meanwhile the sub index c shows the invariance of $\boldsymbol{r}$ with respect of the derivation. The experimental results may be used to relate energy and vorticity for the different non-dimensional parameters. So far the simulations only model the very low Richardson number experiments, which are the least 2D types of flows, but the size growth is similar.

6. – Conclusions

We have developed a three-dimensional model for the study of the turbulence based conceptually on the relation between turbulent vorticity and turbulent velocity. In the same way we have obtained the systems of equations of motion and of energy highlighting the presence of turbulent vorticity components and their transport. The system of equations based on the simplest case (perfect fluid) to a more realistic turbulent model using Reynolds's hypothesis of decomposition has been used and integrated using finite differences. This integration is proposed through three phases. In the first one we evolve, from the initial values of a simple vortex, the second phase is solved by means of the use of the equations of Navier-Stokes and of the vorticity turbulent equations. The dispersion originated in the results of the model by these equations grows very fast, probably due to numerical errors. The third phase begins in step 23 and continues till step 400. The equations used in this third phase correspond exclusively with the proposals for turbulent flow with the inclusion of Reynolds's decomposition. One of the new implementations of this model consists in using as point values the ones that are obtained when the basic equations for turbulent flow are solved, while their average values are always obtained as temporal average using the nine previous temporal values plus the present temporal value, also averaged in space, thus for every point in the mesh that has been discretized using a 3D Cartesian grid of $60 \times 60 \times 120$. Then each of the points covers a spatial and temporal turbulent array of about 5000 points. The temporal integration has been showed throughout three different temporal phases as the turbulence imposes over the laminar regimen growth (Navier-Stokes equations). The related average terms have to be calculated through spatial average. At the second phase, some of those spatial calculations are substituted by the vorticity system of equations. Finally, at the third integration interval (last phase), we have proposed the use of temporal averages together with this system of equation in order to evaluate the instantaneous terms [17].

The laboratory experiments, performed with a grid traversing a quasi–two-dimensional stratified flow, allow to measure also the evolution of the complex vorticity field and show some common features with the numerical experiments based on the proposed vorticity equations. One of the experimental features observed are the non-local behaviour of the large vortices, this could be interpreted as due to the vortical-wave type of interaction [19].

In the simulations different vortices, in order to study the resolution of the problem, have been placed in the central zone of the numerical domain. The results of the flow evolutions are showed through a series of figures of velocity and vorticity fluctuations that allow to explain some topological aspects of the eddies; for instance, their increase in volume, their elongation along their motion, or the appearance of wave patterns, which are not yet clear.

The main variables that have been used to show the behaviour and evolution of the effect of the vortex have been the three components of velocity, three components of average vorticity, the potential temperature and the turbulent perturbations of all of them. In the simulations horizontal planes a symmetry appears on the right-hand and

left-hand side of the first bisecting line of the numerical domain, however the samples in vertical planes present different zones of alteration without any symmetry [20].

The variables with turbulent perturbation or indicating high turbulent vorticity, definitely are able to discriminate the zones of turbulence from the rest of alterations that the vortex produces. The temporal evolution of the elongation of the affected zones by the development of the vortex for the three components of velocity show that the horizontal length suffers an increase 11% of its initial size each time step. The vertical elongation is much smaller because the vertical transport and fluctuations, modelling a stratified flow, are only about 10% of the horizontal ones.

* * *

REFERENCES

[1] Taylor G. I., *Proc. R. Soc. London, Ser. A*, **135** (1931) 685.
[2] Ding F., Arya S. P. and Lin Y.-L., *Env. Fluid. Mech.*, **1** (2001) 29.
[3] Castilla R., Sanchez M. A. and Redondo J. M., *Vortical structures in stratified turbulent flows*, in *Turbulent Diffusion in the Environment*, edited by Redondo J. M. and Babiano A. (FRAGMA) 1993, p. 113.
[4] Arakawa A., *J. Comput. Phys.*, **1** (1966) 119.
[5] Hide R., *Q. J. R. Meteorol. Soc.*, **128** (2002) 1759.
[6] Reynolds O., *Philos. Trans. R. Soc. London, Ser. A*, **186** (1894) 123.
[7] Holzäpfel F., Hofbauer T., Darracq D., Moet H., Garmier F. and Ferreira-Gago C., *Aerospace Sci. Technol.*, **7** (2003) 263.
[8] Cuxart J., Morales G., Terradellas E. and Yagüe C., *Boundary-Layer Meteorol.*, **105** (2) (2002) 305.
[9] Cantalapiedra I. R. and Redondo J. M., *Mixing in Geophysical Flows*, edited by Redondo J. M. and Metais O. (International Center for Numerical Methods, CIMNE) 1995, p. 127.
[10] Redondo J. M. and Linden P. F., *Geometrical observations of turbulent density interfaces*, in *The Mathematics of Deforming Surfaces*, edited by Dritschel D. G. and Perkins R. J. (Clarendon Press Oxford) 1996, p. 221.
[11] Dritschel D. G., *J. Comput. Phys.*, **135** (1997) 217.
[12] Hamed A., Basu D. and Das K., *Comput. Fluids*, **36** (2007) 924.
[13] Matulka A., Carrillo A. and Redondo J. M., these proceedings.
[14] Benoit R., Desgagné M., Pellerin P., Pellerin S. and Chartier Y., *Mon. Weather Rev.*, **125** (1997) 2382.
[15] Oh W. S., Kim J. S. and Kwon O. J., *Comput. Fluids*, **32** (2003) 727.
[16] Shapiro A., *Mon. Weather Rev.*, **121** (1993) 2420.
[17] Cano D., *Turbulent Modelization based on Vorticity*. PhD. Thesis, Univ. Complutense, Madrid (2008).
[18] Derbyshire S. and Redondo J. M., *Anal. Fis.*, **86** (1990) 67.
[19] Gonzalez-Nieto P. L., Cano J. L. and Redondo J. M., *Nuovo Cimento C*, these proceedings.
[20] Redondo J. M., *Vertical microstructure and mixing in stratified flows*, in *Advances in Turbulence*, Vol. **IV**, edited by Gavrilakis S. *et al.* (Kluwer) 1996, p. 605.